ACS APPLIED MATERIALS & INTERFACES

Letter

Cite This: ACS Appl. Mater. Interfaces XXXX, XXX, XXX−XXX

www.acsami.org

# *In Situ* Active Poling of Nanofiber Networks for Gigantically Enhanced Particulate Filtration

Chun Xiao Li,[†,‡] Shuang Yang Kuang,[†,‡] Yang Hui Chen,[†,‡] Zhong Lin Wang,[†,‡,¶,#] Congju Li,[†,‡] and Guang Zhu*[,†,‡,§,∥]

[†]CAS Center for Excellence in Nanoscience, Beijing Key Laboratory of Micro-Nano Energy and Sensor, Beijing Institute of Nanoenergy and Nanosystems, Chinese Academy of Sciences, Beijing 100083, China

[‡]School of Nanoscience and Technology, University of Chinese Academy of Sciences, Beijing 100049, China

[§]Department of Mechanical, Materials and Manufacturing Engineering, The University of Nottingham Ningbo China, Ningbo 315100, China

[∥]New Materials Institute, The University of Nottingham Ningbo China, Ningbo 315100, China

[¶]Center on Nanoenergy Research, School of Physical Science and Technology, Guangxi University, Nanning 530004, China

[#]School of Materials Science and Engineering, Georgia Institute of Technology, Atlanta, Georgia 30332, United States

Supporting Information

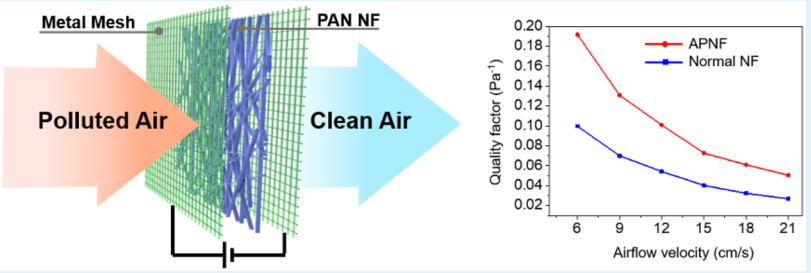


**ABSTRACT:** Enhancing the filtration efficiency of air filtering material without increasing its airflow resistance is a major challenge and of great significance. In this work, we report a type of active-poled nanofiber onto which *in situ* active poling is applied. It results in significantly enhanced filtration efficiency as well as dust holding capacity while keeping the airflow resistance constant. Owing to the *in situ* applied electric field, the nanofibers as well as the particulates are polarized. As a result, at a poling voltage of 2 kV, the removal efficiency and the quality factor for $PM_{2.5}$ are enhanced by 17% and 130%, respectively. More importantly, the dust holding capacity represents a 3.5-fold enhancement over normal nanofibers. The approach reported in this work has the potential of being practically utilized in air purification purposes because it can bring about not only promoted filtration performance but also lowered noise and reduced power consumption.

**KEYWORDS:** *air filtering material, in situ active poling, active-poled nanofibers, filtration efficiency, dust holding capacity*

## 1. INTRODUCTION

Air filtering materials aim to intercept and capture solid particulates such as dust, pollen, bacteria, and particulate matter (PM) pollutant.[1−3] The demand on the air filtering materials in recent years has been substantially increasing on a worldwide scale because people are paying extensive attention to $PM_{2.5}$ pollution,[3−5] which consists of fine inhalable and noxious pollutant particles with diameters generally smaller than 2.5 $\mu$m,[6,7] and $PM_{10}$ refers to particles less than 10 $\mu$m in diameter.[6,7] For decades, the development of air filtering materials has been always focused on how to achieve high filtration efficiency but at low airflow resistance, which is challenging because of the trade-off between these two pivotal characters.[1,3] In recent years, electrospun polymer nanofibers have emerged as promising materials for air filtration[8−11] due to nanoscaled air space between fibers, large specific surface area, and strong van der Waals[12] force. Gong et al. found that thinner nanofibers were more efficient in capturing $PM_{2.5}$ owing to stronger van der Waals force.[12−14] Liu et al. revealed that nanofibers made of materials with polar functional groups exhibited higher removal efficiency for $PM_{2.5}$.[15,16] Zhang et al. prepared hierarchical nanostructured nanofibers[17] and electret nanofibers[18] to increase the filtration efficiency. Despite these advances, major challenges still exist. Electrospun nanofibers are normally densely packed with little three-dimensional space.[19] The compact structure does not favor reducing the airflow resistance while still maintaining high filtration efficiency.[20] Furthermore, the compactness also causes undesirable dust holding capacity because the airflow pathways

Received: May 3, 2018
Accepted: July 2, 2018
Published: July 6, 2018






DOI: 10.1021/acsami.8b07203
ACS Appl. Mater. Interfaces XXXX, XXX, XXX−XXX

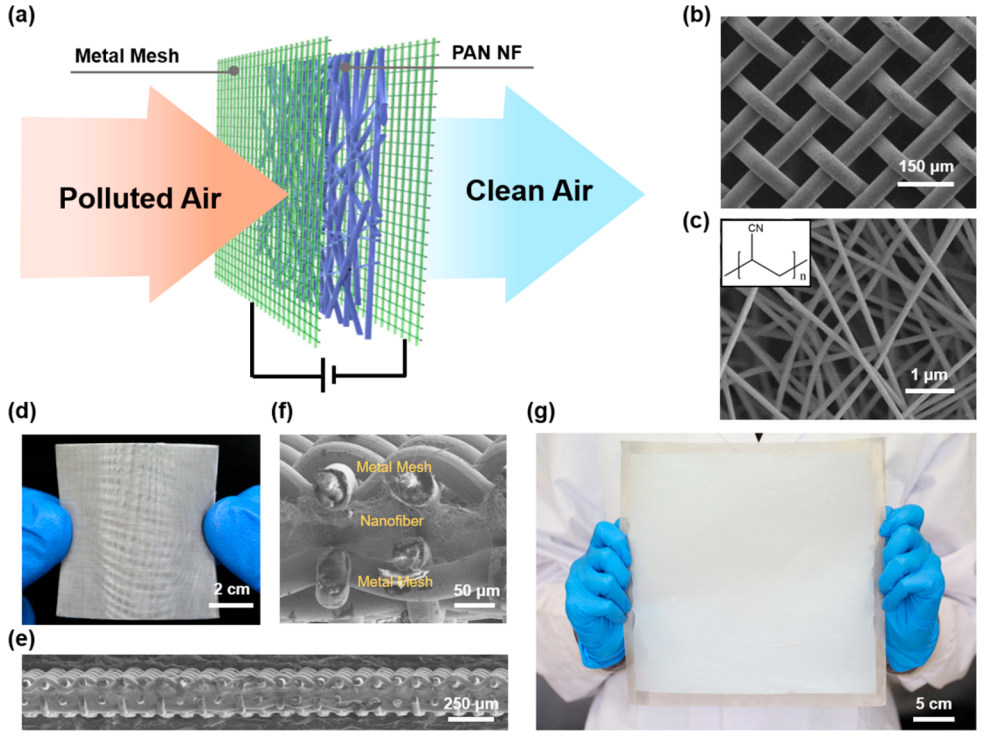


**Figure 1.** Structure of the active-poled nanofibers (APNFs). (a) Schematic showing the basic structure of the APNF. (b) SEM image of the 200 mesh metal network. (c) SEM image of the electrospun PAN nanofibers. The inset shows the molecular formula of PAN. (d) Photograph of the APNF in a small piece. (e) Cross-sectional view of the APNF in a SEM image. (f) Enlarged view of the APNF's cross section in a SEM image. (g) Photograph of the APNF in a large area.

are subject to be clogged up by the particulates,[1,21] which then results in short service life of the nanofiber-based filters.

In this work, we report a type of active-poled nanofibers (APNF) onto which *in situ* poling is applied, resulting in significantly enhanced filtration efficiency as well as dust holding capacity without increasing airflow resistance. Polyacrylonitrile (PAN) based nanofibers are sandwiched between two layers of metal network. As a voltage is applied across the metal layers, the nanofibers are polarized by the electric field. Meanwhile, neutral particulates that are passing through the nanofibers also become polarized. As a result, electrostatic attraction, which is a type of long-range force,[22,23] effectively seizes the particulates onto the nanofibers. At an airflow velocity of 0.21 m/s and a poling voltage of 2k volts, the removal efficiency for $PM_{2.5}$ reaches 98.72% compared to 84.41% for the case without the poling, while the airflow resistance remains constant. Correspondingly, the quality factor presents a 130% enhancement from 0.023 $Pa^{-1}$ to 0.053 $Pa^{-1}$. The dust holding capacity is found to be 8.43 g/$m^2$, representing over 3-fold enhancement as normal PAN nanofibers only have a dust holding capacity of 2.41 g/$m^2$. In general, the APNF appropriately addresses the aforementioned concerns of using electrospun nanofibers (NFs) for air filtration. If it is adopted in air purification equipment, it is promising to bring about advantages including greatly promoted purification speed, lowered noise, reduced power consumption, and extended service life.

## 2. RESULTS AND DISCUSSION

The basic structure of the APNF is schemed in Figure 1a. Two layers of metal network clamp a layer of electrospun nanofibers in between. A dc voltage source is loaded across the metal layers. Airflow is driven through the nanofibers by an electric fan. The scanning electron microscope (SEM) image of the metal network made of steel is shown in Figure 1b. With mesh grade of 200, the wire diameter is 50 $\mu$m, and the pore size is 80 $\mu$m. The SEM image of the PAN nanofibers is presented in Figure 1c, which exhibits nonwoven characteristic and a uniform diameter of about 200 nm (Figure S1a). Additionally, the pore size of the PAN nanofibers shows a well-developed peak centered at 10.8 $\mu$m (Figure S1b), and the porosity reaches up to 96.43%. The inset in Figure 1c illustrates the PAN molecular formula that possesses a strong polar functional group (C−N). This feature favors polarization as well as filtration efficiency[17,18] which will be evidenced in the following session. The top-down view of the multilayered structure is displayed by a photograph in Figure 1d. The sandwiched lamination is further revealed in detail by cross-sectional views in Figure 1e and Figure 1f. The overall thickness of the structure is found to be 250 $\mu$m. Large area samples can also be prepared, as proved by the 25 × 25 $cm^2$ sample shown in Figure 1g. The detailed fabrication process is discussed in the Experimental Section (Supporting Information).

Here, the experimental setup for assessing the filtering performance consists of two individual glass chambers that are connected by the APNF, two particle counters that measure the $PM_{2.5}$ concentration on the opposite sides of the APNF, and a fan that drives the airflow. The particulate source was generated by burning cigarettes.[15,16] It was proved that cigarette smoke resembles haze pollutant in terms of composition and surface chemistry.[16] Here the smoke was dispersed in a 2 $m^3$ acrylic-based enclosed chamber, and all tests were performed with the $PM_{2.5}$ mass concentration higher


DOI: 10.1021/acsami.8b07203
ACS Appl. Mater. Interfaces XXXX, XXX, XXX−XXX

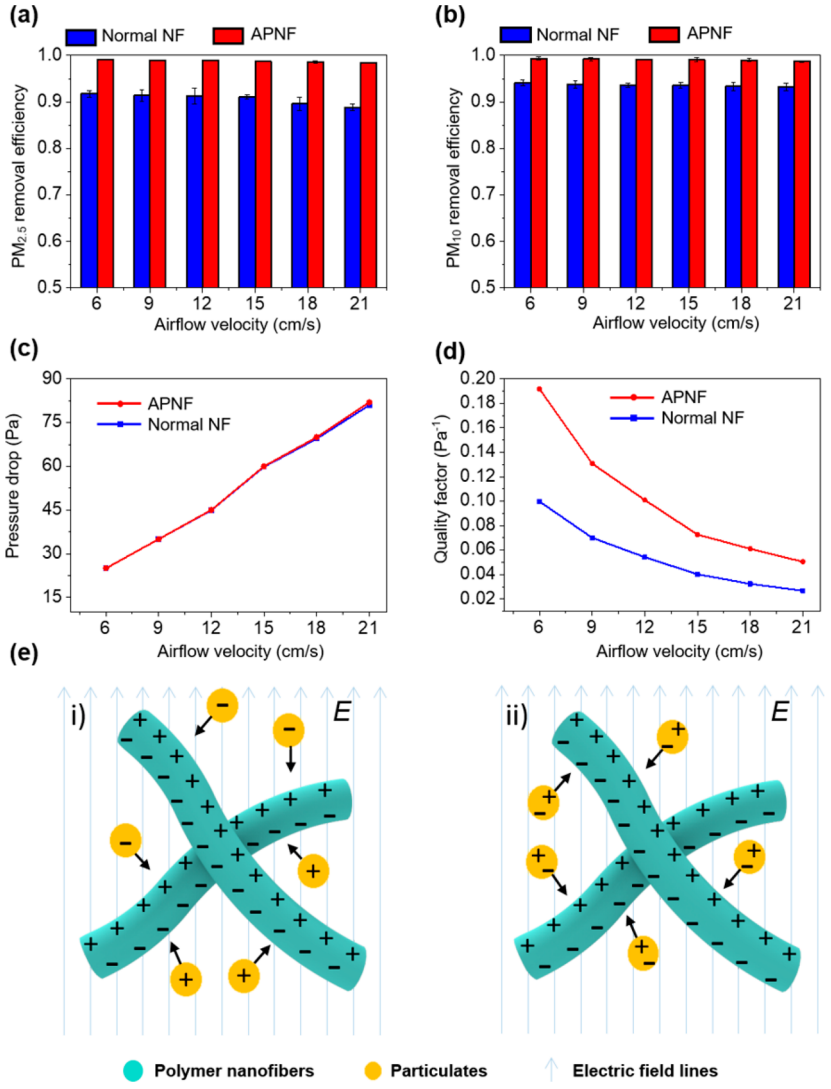


**Figure 2.** Filtration performance of the APNF and the normal nanofibers (NFs) at different airflow velocity, (a) $PM_{2.5}$ removal efficiency, (b) $PM_{10}$ removal efficiency, (c) pressure drop, and (d) quality factor from both the APNF and the normal NF at different airflow velocity. Error bar represents the standard deviation of three replicate measurements. (e) The mechanism of the APNF for capturing particulates. (i), (ii) Schematic diagrams that illustrate the process of capturing charged and neutral particulates, respectively.

than 300 $\mu g/m^3$ prior to the filtration. The detailed structure of the experimental setup is photographed in Figure S2.

The removal efficiency here is calculated by the following eq 1[24−26]

$$E = (C_0 - C)/C_0 \quad (1)$$

where $E$ represents the removal efficiency, and $C_0$ ($\mu g/m^3$) and $C$ ($\mu g/m^3$) are the measured particulate mass concentrations prior to and after the filtration, respectively. The quantified $PM_{2.5}$ and $PM_{10}$ removal efficiencies under different airflow velocity are presented in Figure 2a and Figure 2b, respectively. It is explicitly revealed that the removal efficiency for $PM_{2.5}$ with a 2 kV poling voltage is significantly enhanced compared to that from normal nanofibers without the poling. At an airflow velocity of 0.21 m/s, the $PM_{2.5}$ removal efficiency is promoted from 88.81% to 98.41%, and the $PM_{10}$ removal efficiency also increases from 93.21% to 98.72%. It is noticed that the removal efficiency decreases as the airflow velocity increases, which is a common nature of filtering materials.[18] When the airflow velocity increases from 0.06 to 0.21 m/s, the $PM_{2.5}$ removal efficiency of normal nanofibers decreases by 2.87%. In contrast, the APNF presents a drop by only 0.77% in the removal efficiency. Similar observation was also obtained for the $PM_{10}$ removal. This feature proves the robustness of the APNF against high airflow, which is crucial for high-standard purification purposes.

Apart from the removal efficiency, the airflow resistance is another key parameter to assess the performance of air filtering materials. Here, pressure drop through the APNF is adopted to quantitatively represent the airflow resistance. As shown in Figure 2c, the pressure drop is positively correlated with the airflow velocity. It is found that the pressure drop of the APNF as well as the normal nanofibers is the same at 82 Pa with the airflow velocity of 0.21 m/s, indicating that the metal layers hardly cause additional pressure drop. As a result, we can calculate the quality factor (QF) of filtering materials according to eq 2 below[16]

$$QF = -\ln(1 - E\%)/\Delta P \quad (2)$$

where $E$ and $\Delta P$ represent the removal efficiency and the pressure drop, respectively. As outlined in Figure 2d, the QF



DOI: 10.1021/acsami.8b07203
ACS Appl. Mater. Interfaces XXXX, XXX, XXX−XXX

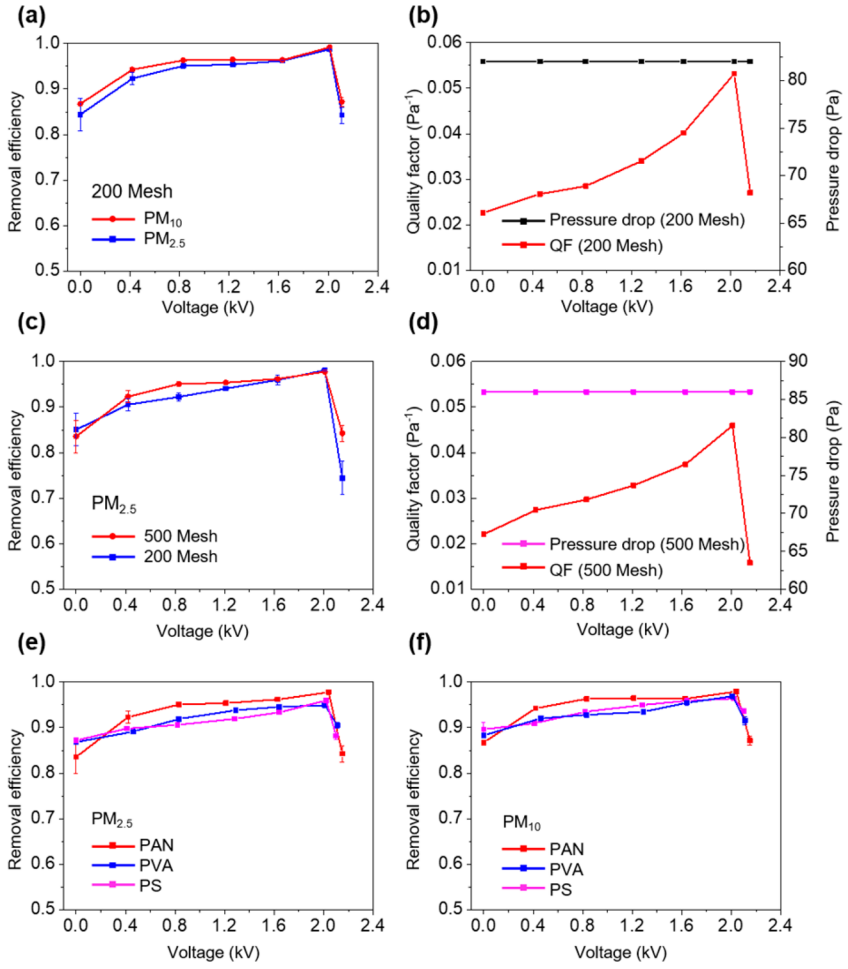


**Figure 3.** Filtration performance at different poling voltages. (a) The correlation between the PM removal efficiency of the APNF (with 200 mesh grade) and the poling voltage. (b) Pressure drop and quality factor of the APNF (with 200 mesh grade for $PM_{2.5}$) at different poling voltages. (c) The correlation between the PM removal efficiency of the APNF (with 500 mesh grade) and the poling voltage. (d) Pressure drop and quality factor of the APNF (with 500 mesh grade for $PM_{2.5}$) at different poling voltages. (e) $PM_{2.5}$ and (f) $PM_{10}$ removal efficiency of the APNF based on three different materials as affected by the poling voltage. All of the tests were conducted at a constant airflow velocity of 0.21 m/s. Error bar represents the standard deviation of three replicate measurements.

values of the APNF are doubled compared to those of normal nanofiber (NF). At the airflow velocity of 0.21 m/s, the APNF with a 2 kV poling voltage has a significantly high QF value of 0.053 $Pa^{-1}$ (shown in Table S1). It is worth noting that this value is 2 to 3 times higher compared to recently reported state-of-the-art results based on nanofibers.[15,16]

The observed enhancement originates from the applied electric field in two likely scenarios, as illustrated in Figure 2e. Once a poling voltage is loaded, the electric field across the metal layers reaches up to the order of tens of MV/m. As a result, the PAN-based nanofibers become polarized, forming polarized surface charges.[27] Consequently, provided that the incoming particulates carry net charges, they are then attracted to the fiber surface as passing by due to electrostatic interaction (Figure 2e-i).[28] Even if the particulates are neutral, they are instantaneously polarized once entering the electric field zone, as shown in Figure 2e-ii.[27] Then the dipole−dipole interaction leads to the deposition of the polarized particulates onto the nanofibers.

Following the proposed mechanism above, we investigated the correlation between the applied voltage and the removal efficiency. As shown in Figure 3a, the poling voltage plays a crucial role in manipulating the removal efficiency for both $PM_{2.5}$ and $PM_{10}$. Below an optimal value of 2 kV, higher voltage corresponds to incremental improvement of the removal efficiency. This can be well explained by the aforementioned mechanism, in which higher voltage generates more polarized surface charges and thus stronger electrostatic attraction. However, if the voltage exceeds the optimal value of 2 kV, the removal efficiency significantly plumps. As the pressure drop is found to be independent of the applied voltage, the QF then experiences a substantial rise and then a sharp drop, as presented in Figure 3b. This phenomenon is most likely attributed to air breakdown resulting from excessively high voltage. Once the air breakdown occurs, the electric field strength is no longer maintained, leading to much weakened polarization. Besides, the electric discharging that accompanies the air breakdown is likely to cause structural damage to the nanofibers and then compromise the removal efficiency. It is worth noting that the APFN at the optimal poling voltage does not involve air breakdown. As a result, no hazardous ozone gas will be generated, which differentiates the APFN from conventional air purification means of negative ions.[29]

Two designing factors that influence the filtration performance were then examined. The first factor is the mesh density


DOI: 10.1021/acsami.8b07203
ACS Appl. Mater. Interfaces XXXX, XXX, XXX−XXX

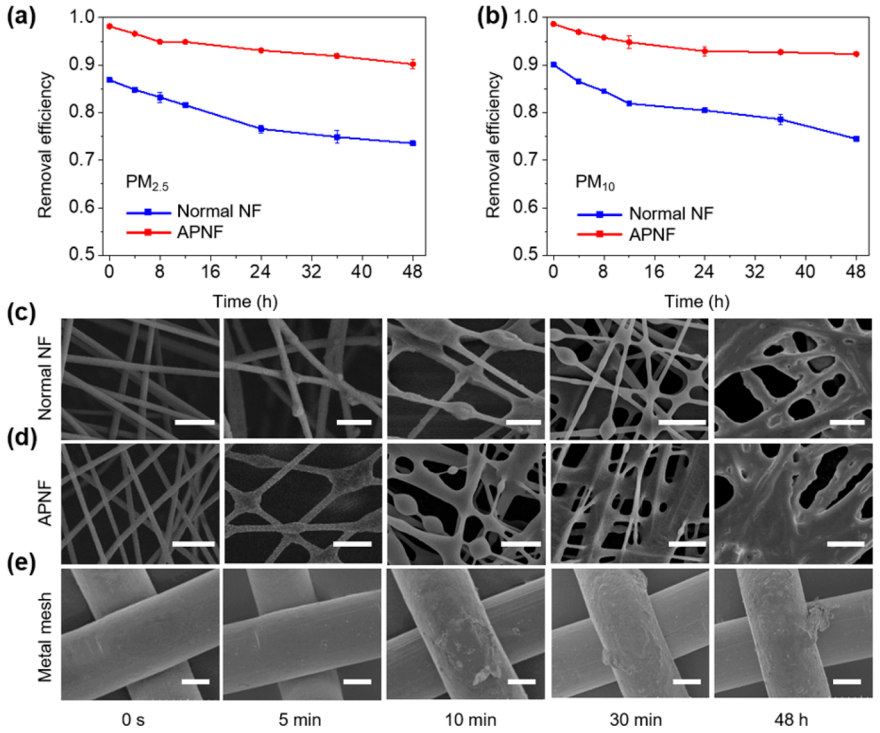


**Figure 4.** Filtration performance by long-time test. (a), (b) The relation between time and the removal efficiency for $PM_{2.5}$ and $PM_{10}$, respectively, from both the APNF and the normal NF. (c), (d), (e) Microscopic morphologies of the normal NF, the APNF, and the metal mesh in top-down viewed SEM images at different time points during the test, respectively; the scale bars represent 5 $\mu$m, 5 $\mu$m, and 20 $\mu$m, respectively. All of the tests were conducted at a constant airflow velocity of 0.21 m/s. Error bar represents the standard deviation of three replicate measurements.

of the metal network. As demonstrated in Figure 3c, the metal network with different mesh density (i.e., mesh grade 200 and mesh grade 500, SEM image shown in Figure S3) exhibits similar removal efficiency as the poling voltage increases. This is because the electric field generated by the two types of metal networks is equally uniform, which is proved by the numerical simulation results in Figure S4. However, due to smaller pore size, the 500-grade mesh exhibits greater pressure drop as compared to the 200-grade mesh (Figure 3d). As a result, the 500-grade mesh APNF presents inferior QF values (Figure 3d), which explains the adoption of the 200-grade mesh in this work.

The second critical factor that affects the filtration performance is the material of the nanofibers, which correlates to the surface charges resulting from the poling. To illustrate this point, we selected three types of materials to fabricate the nanofibers, including PAN, polystyrene (PS), and poly(vinyl alcohol) (PVA). Their calculated dipole moments for the repeating units vary to a great extent, i.e., 3.6, 0.7, and 1.2 D, respectively.[16] The molecular models and the SEM images of the three materials are shown in Figure S5. The detailed process for preparing the nanofibers of different materials that have equal average diameter of 200 nm is shown in the Experimental Section (SI). Figure 3e and Figure 3f exhibit the removal efficiency for $PM_{2.5}$ and $PM_{10}$ from the APNF made of the three materials, respectively. Two major observations were obtained. On one hand, for all of the three materials, the removal efficiency unanimously increases as the poling voltage is loaded, showing a positive correlation. This is because surface polarization is a common nature of polymers within an electric field. On the other hand, the extent of the efficiency enhancement differs among the three materials. The most prominent improvement (i.e., 12.3%) comes from the PAN-based nanofibers, which have the highest dipole moment. In contrast, the efficiency enhancement is found to be only 8.5% for the PS-based nanofibers that have the weakest dipole moment. Besides, we used commercial meltblown nonwovens as the filtering layer for comparison, observing that the enhancement of the filtration efficiency is insignificant from 90.45% to 91.51% for $PM_{2.5}$. This is probably attributed to the fact that polypropylene is a type of nonpolar polymer. As a result, the polarized charges induced on the polypropylene fibers are much weaker than the polar PAN nanofibers. Therefore, in order to demonstrate the *in situ* poling effect, the PAN nanofibers were selected. In addition, the influence of the nanofiber thickness on the removal efficiency was also investigated with data shown in Figure S6 and Table S2. It is obtained that the APNF with the thickness of 13.0 $\mu$m presents the optimal overall filtration performance with the highest QF (shown in Table S2).

To reveal the superiority of the APNF in terms of service life, dust holding capacity was obtained through a long-time test. During the test, the ambient $PM_{2.5}$ concentration prior to filtration was kept stable. The dust holding capacity refers to the mass of the captured particulates per unit area as the removal efficiency degrades to 85% of the initial removal efficiency. Then, the dust holding capacity is calculated by the following eq 3[24,25]

$$\Delta m = (m - m_0)/S \tag{3}$$

where $m$ (g) and $m_0$ (g) are the mass of the APNF after and before the long-time test, respectively, and $S$ ($m^2$) is the surface area of the APNF. The test was conducted at the constant airflow velocity of 0.21 m/s. After 48 h, the $PM_{2.5}$ removal efficiency of the normal nanofibers reduces from 86.85% to 73.56% (Figure 4a), representing a 15% reduction compared


DOI: 10.1021/acsami.8b07203
ACS Appl. Mater. Interfaces XXXX, XXX, XXX−XXX

to the initial efficiency and indicating the failure of the filtering material. Based on eq 3, the dust holding capacity of the normal PAN nanofibers is calculated to be 2.41 g/m$^2$. In contrast, the APNF with the 2 kV poling exhibits a drop of the removal efficiency from 98.15% to 90.18% after 48 h. With only 7% efficiency reduction compared to the initial value, the APNF is still functional without failure. After further test, the dust holding capacity of the APNF was then found to be 8.43 g/m$^2$. Therefore, the APNF proves to have significantly superior dust holding capacity with more than 3-fold enhancement in comparison to the normal nanofibers. Similar results were also obtained for the $PM_{10}$ removal. The SEM images in Figure 4c–e present the morphology evolution of the normal nanofibers, the APNF, and the metal mesh as the captured particulates accumulate, respectively. Regardless of the poling, the captured particulates tend to bond tightly onto the nanofibers and gradually aggregate to form larger particles at the junctions of the nanofibers. As the particulates accumulate, the nanofibers are subject to be clogged up, which is consistent with previous observations in the literature.[1,21] From the SEM images, it can be explicitly obtained that the APNF can capture apparently more particulates than the normal nanofibers within the same time frame. Even though the APNF has captured more particulates, it still presents higher removal efficiency, which is attributed to the *in situ* poling. Besides, it is worth mentioning that most of the particulates captured by the APNF are deposited onto the nanofibers instead of the metal mesh (Figure 4e), which rules out the possibility that the removal efficiency enhancement may originate from the electrically charged metal layers.

## 3. CONCLUSIONS

The proved features of the APNF indicate significance for real applications in air purification equipment. First, without adding the airflow resistance, the APNF can result in higher removal efficiency while keeping the airflow constant. As a consequence, it can generate a higher clean air delivery rate, which is normally abbreviated as CADR, a key parameter for air purifiers. Here, CADR can be obtained using the following eq 4[30]

$$\mathrm{CADR} = E \times L \times R \tag{4}$$

where $E$ and $L$ represent the single-pass removal efficiency and the airflow rate, respectively, and $R$ represents the short-circuit factor ($R$ = 1 under well-mixed conditions). In general, $L$ and $R$ are constants in the same air filtration testing condition. Then, the CADR is positively correlated with the single-pass removal efficiency $E$. As a result, air filters using the APFN are expected to yield a CADR enhancement of 17% based on the obtained results above. Second, because the APNF possesses enhanced removal efficiency, the airflow can be sacrificed, while the CADR is still kept constant. The reduced airflow then will bring about lowered wind noise and saved power consumption from the electric fan. Moreover, the multifold increase of the dust holding capacity apparently favors the service life of the air filters. Then, consumable cost as well as maintenance cost are expected to be saved by over 70%.

In summary, we developed an APNF that possesses significantly enhanced filtration efficiency and dust holding capacity without increasing the pressure drop of normal nanofibers. Owing to the *in situ* applied electric field, the nanofibers as well as the particulates are polarized, leading to gigantically promoted filtration performance. At the poling voltage of 2 kV, the removal efficiency, the quality factor, and the dust holding capacity for $PM_{2.5}$ are enhanced by 17%, 130%, and 250%, respectively. More importantly, the fabrication process of the APNF is compatible to large area roll-to-roll manufacturing and can be potentially made into air filters. If used for air purification purposes, the air filters that utilize the APNF have prominent advantages including promoted purification speed, lowered noise, reduced power consumption, and extended service life.

## ■ ASSOCIATED CONTENT

### Supporting Information

The Supporting Information is available free of charge on the ACS Publications website at DOI: 10.1021/acsami.8b07203.

Experimental Section; Fiber diameter distribution and pore size distribution of the electrospun PAN nanofibers (Figure S1); Photograph of the experimental setup for characterizing the filtering materials (Figure S2); SEM images of the metal layers (Figure S3); Electric field distribution obtained by COMSOL numerical simulation (Figure S4); Molecular models and SEM images of different polar polymers (Figure S5); The thickness of the electrospun PAN nanofibers (Figure S6); Table S1: The filtration performance of the APNF compared with the normal nanofibers at the airflow velocity of 0.21 m/s; Table S2: The filtration performance of the APNF and the normal PAN nanofibers as affected by the thickness at the airflow velocity of 0.21 m/s (PDF)

## ■ AUTHOR INFORMATION


### Corresponding Author

*E-mail: zhuguang@binn.cas.cn (G.Z.).

### ORCID

Guang Zhu: 0000-0003-2350-0369


### Author Contributions

Experiments were conceived and designed by G.Z. and C.X.L. The experimental setup was constructed by C.X.L and S.Y.K. C.X.L did the measurements and collected the data. Y.H.C. and C.X.L. took photographs in the figures. C.X.L. and G.Z. analyzed the data and cowrote the manuscript. C.L. and Z.L.W. amended the manuscript. All of the authors discussed and proofread the manuscript.

### Notes

The authors declare no competing financial interest.

## ■ ACKNOWLEDGMENTS

This research was supported by the National Key R&D Project from Ministry of Science and Technology, China (Grant No. 2016YFA0202701&2016YFA0202703), National Science Foundation of China (Grant No. 51572030), Beijing Natural Science Foundation (Grant No. 2162047), and China Thousand Talents Program.

## ■ REFERENCES

(1) Li, P.; Wang, C.; Zhang, Y.; Wei, F. Air Filtration in the Free Molecular Flow Regime: a Review of High-Efficiency Particulate Air Filters Based on Carbon Nanotubes. *Small* **2014**, *22*, 4543–4561.

(2) Huang, R.-J.; Zhang, Y.; Bozzetti, C.; Ho, K.-F.; Cao, J.-J.; Han, Y.; Daellenbach, K. R.; Slowik, J. G.; Platt, S. M.; Canonaco, F.; et al. High Secondary Aerosol Contribution to Particulate Pollution During Haze Events in China. *Nature* **2014**, *514*, 218–222.



DOI: 10.1021/acsami.8b07203
ACS Appl. Mater. Interfaces XXXX, XXX, XXX–XXX

(3) Hinds, W. C. *Aerosol Technology: Properties, Behavior, and Measurement of Airborne Particles*; Wiley: New York, 1982.
(4) Nel, A. Air Pollution-Related Illness: Effects of Particles. *Science* **2005**, *308*, 804−806.
(5) Sheehan, P.; Cheng, E.; English, A.; Sun, F. China's Response to the Air Pollution Shock. *Nat. Clim. Change* **2014**, *4*, 306−309.
(6) Lelieveld, J.; Evans, J. S.; Fnais, M.; Giannadaki, D.; Pozzer, A. The Contribution of Outdoor Air Pollution Sources to Premature Mortality on a Global Scale. *Nature* **2015**, *525*, 367−371.
(7) Shindell, D.; Kuylenstierna, J. C. I.; Vignati, E.; Dingenen, R. V.; Amann, M.; Klimont, Z.; Anenberg, S. C.; Muller, N.; Janssens-Maenhout, G.; Raes, F.; et al. Simultaneously Mitigating Near-term Climate Change and Improving Human Health and Food Security. *Science* **2012**, *335*, 183−189.
(8) Huang, Z. M.; Zhang, Y. Z.; Kotaki, M.; Ramakrishna, S. A Review on Polymer Nanofibers by Electrospinning and Their Applications in Nanocomposites. *Compos. Sci. Technol.* **2003**, *63*, 2223−2253.
(9) Greiner, A.; Wendorff, J. H. Electrospinning: a Fascinating Method for the Preparation of Ultrathin Fibers. *Angew. Chem., Int. Ed.* **2007**, *46*, 5670−5703.
(10) Li, D.; Xia, Y. N. Electrospinning of Nanofibers: Reinventing the Wheel? *Adv. Mater.* **2004**, *16*, 1151−1170.
(11) Thavasi, V.; Singh, G.; Ramakrishna, S. Electrospun Nanofibers in Energy and Environmental Applications. *Energy Environ. Sci.* **2008**, *1*, 205−221.
(12) Shi, Q.; Wan, K. T.; Wong, S. C.; Chen, P.; Blackledge, T. A. Do Electrospun Polymer Fibers Stick? *Langmuir* **2010**, *26*, 14188−14193.
(13) Gong, G.; Zhou, C.; Wu, J.; Jin, X.; Jiang, L. Nanofibrous Adhesion: the Twin of Gecko Adhesion. *ACS Nano* **2015**, *9*, 3721−3727.
(14) Autumn, K.; Liang, Y. A.; Tonia Hsieh, S.; Zesch, W.; Chan, W. P.; Kenny, T. W.; Fearing, R.; Full, R. J. Adhesive Force of a Single Gecko Foot-Hair. *Nature* **2002**, *405*, 681−685.
(15) Zhang, R. F.; Liu, C.; Hsu, P.-C.; Zhang, C. F.; Liu, N.; Zhang, J. S.; Lee, H. R.; Lu, Y. Y.; Qiu, Y. C.; Chu, S.; et al. Nanofiber Air Filters with High-Temperature Stability for Efficient $PM_{2.5}$ Removal from the Pollution Sources. *Nano Lett.* **2016**, *16*, 3642−3649.
(16) Liu, C.; Hsu, P.-C.; Lee, H.-W.; Ye, M.; Zheng, G. Y.; Liu, N.; Li, W. Y.; Cui, Y. Transparent Air Filter for High-Efficiency $PM_{2.5}$ Capture. *Nat. Commun.* **2015**, *6*, 6205.
(17) Zhang, S. C.; Tang, N.; Cao, L.; Yin, X.; Yu, J. Y.; Ding, B. Highly Integrated Polysulfone/Polyacrylonitrile/Polyamide-6 Air Filter for Multi-Level Physical Sieving Airborne Particles. *ACS Appl. Mater. Interfaces* **2016**, *8*, 29062−29072.
(18) Wang, S.; Zhao, X. L.; Yin, X.; Yu, J. Y.; Ding, B. Electret Polyvinylidene Fluoride Nanofibers Hybridized by Polytetrafluoroethylene Nanoparticles for High-Efficiency Air Filtration. *ACS Appl. Mater. Interfaces* **2016**, *8*, 23985−23994.
(19) Zhang, S. C.; Liu, H.; Yu, J. Y.; Luo, W. J.; Ding, B. Microwave Structured Polyamide-6 Nanofiber/net Membrane with Embedded poly(m-phenylene isophthalamide) Staple Fibers for Effective Ultrafine Particle Filtration. *J. Mater. Chem. A* **2016**, *4*, 6149−6157.
(20) Zuo, F. L.; Zhang, S. C.; Liu, H.; Fong, H.; Yin, X.; Yu, J. Y.; Ding, B. Free-Standing Polyurethane Nanofiber/nets Air Filters for Effective PM Capture. *Small* **2017**, *13*, 1702139.
(21) Leung, W.W.-F.; Hung, C.-H. Skin Effect in Nanofiber Filtration of Submicron Aecrosols. *Sep. Purif. Technol.* **2012**, *92*, 174−180.
(22) Jeong, S.; Cho, H.; Han, S.; Won, P.; Lee, H.; Hong, S.; Yeo, J.; Kwon, J.; Ko, S. H. High Efficiency, Transparent, Reusable, and Active $PM_{2.5}$ Filters by Hierarchical Ag Nanowire Percolation Network. *Nano Lett.* **2017**, *17*, 4339−4346.
(23) Cheng, Y. L.; Wang, C. Y.; Zhong, J. W.; Lin, S. Z.; Xiao, Y. J.; Zhong, Q. Z.; Jiang, H. L.; Wu, N.; Li, W. B.; Chen, S. W.; et al. Electrospun Polyetherimide Electret Nonwoven for Bi-functional Smart Face Mask. *Nano Energy* **2017**, *34*, 562−569.
(24) Zhang, Y. Y.; Yuan, S.; Feng, X.; Li, H. W.; Zhou, J. W.; Wang, B. Preparation of Nanofibrous Metal-Organic Framework Filters for Efficient Air Pollution Control. *J. Am. Chem. Soc.* **2016**, *138*, 5785−5788.
(25) Chen, Y. F.; Zhang, S. H.; Cao, S. J.; Li, S. Q.; Chen, F.; Yuan, S.; Xu, C.; Zhou, J. W.; Feng, X.; Ma, X. J.; Wang, B. Roll-to-Roll Production of Metal-Organic Framework Coatings for Particulate Matter Removal. *Adv. Mater.* **2017**, *29*, 1606221.
(26) Gibson, P.; Schreuder-Gibson, H.; Rivin, D. Transport Properties of Porous Membranes Based on Electrospun Nanofibers. *Colloids Surf., A* **2001**, *187*, 469−481.
(27) Van Turnhout, J. V.; Adamse, J. W. C.; Hoeneveld, W. J. Electret Filters for High-Efficiency Air Cleaning. *J. Electrost.* **1980**, *8*, 369−379.
(28) Tsai, P. P.; Schreuder-Gibson, H.; Gibson, P. Different Electrostatic Methods for Making Electret Filters. *J. Electrost.* **2002**, *54*, 333−341.
(29) Grabarczyk, Z. Effectiveness of Indoor Air Cleaning with Corona Ionizers. *J. Electrost.* **2002**, *51*, 278−283.
(30) Kim, H.-J.; Han, B.; Kim, Y.-J.; Yoon, Y.-H.; Oda, T. Efficient Test Method for Evaluating Gas Removal Performance of Room Air Cleaners Using FTIR Measurement and CADR Calculation. *Building and Environment* **2012**, *47*, 385−393.


DOI: 10.1021/acsami.8b07203
*ACS Appl. Mater. Interfaces* XXXX, XXX, XXX−XXX